

基于偶极子天线辐射反向创建空间球形聚焦光斑

王俊杰, 杨艳芳*, 何英, 李琦, 王昆峰

上海大学理学院物理系, 上海 200444

摘要 与传统的仅能生成光轴方向的球形聚焦光斑不同,本文提出了一种在4Pi聚焦系统中通过反聚焦偶极子天线辐射场产生具有规定空间方向和间距的球形聚焦光斑的方法。该方法是将规定好长度和极化方向的空间偶极子天线置于4Pi聚焦系统的焦点处,通过逆问题解析求解出生成球形聚焦光斑的物镜瞳孔面上的输入场。然后使用瞳孔面处的场,并选择合适的偶极子天线长度,就能获得球形聚焦光斑。数值结果表明,创建的球形聚焦光斑的空间方向与设置的偶极子天线的极化方向一致,球形聚焦光斑之间的距离也等于偶极子天线的长度。本文提出的方法比传统方法更灵活,可以创建具有规定空间位置的球形聚焦光斑,这对空间任意位置捕获纳米粒子具有很大的应用价值。

关键词 物理光学; 球形聚焦光斑; 偶极子天线; 4Pi聚焦系统

中图分类号 O436 文献标志码 A

DOI: 10.3788/AOS231679

1 引言

1986年, Ashkin^[1]通过实验发现,单束激光经过强聚焦得到的辐射压力可以稳定捕获单个粒子。这项技术现在被称为光学捕获或光学镊子^[2-3],可以应用到电介质颗粒^[4]、半导体量子点^[5-6]和金属纳米颗粒^[7-9]的捕获和操作中。多年的研究发现,特殊的光场结构可以应用到光学捕获的微操纵领域,而具有空间非均匀偏振状态的矢量光场(VOF)^[10]的新颖聚焦特性产生许多独特的焦场结构,如光链^[11-12]、光针^[13-14]、光学囚笼^[15]和球形聚焦光斑^[16-17]等。其中,具有同等三维空间分辨率的球形光斑在光学显微镜和金属粒子捕获方面具有重要应用,使得人们尤其关注它。在金属粒子捕获研究中, Zhan等^[18]发现,当捕获非共振金属粒子时,径向偏振光束的强聚焦场有着极强的轴向分量,可提供大的梯度力,还不会产生轴向散射力和吸收力,能形成三维光学陷阱稳定捕获金属粒子。但2011年, Ohlinger等^[19]发现,当捕获共振金属粒子时,因为被显著增加的散射力和严重的光学加热效应破坏,使得光学捕获无法实现。2016年, 芮光浩等^[20]发现,径向偏振光束的4Pi聚焦可形成球形聚焦光斑,其中增强的轴向梯度力和4Pi聚焦系统对称性可抵消的轴向散射力和吸收力,能实现稳定捕获共振条件下的金属粒子,并能精确控制金属离子的运动轨迹。因此多年来,创建多个球形聚焦光斑的方法是一个研究热点,例如, Zhan等^[16]

提出用偶极子天线可以在光轴上生成亮度不同的多个球形聚焦光斑。

然而,据我们所知,目前所有报道生成的球形聚焦光斑都是沿着光轴的。本文将天线辐射理论引入到矢量光场的聚焦领域,提出了一种创建具有规定空间方向和距离的球形聚焦光斑的方法。该方法通过反向4Pi聚焦来自偶极子天线(DA)的辐射场,聚焦形成的球形光斑的位置与在4Pi聚焦系统焦点上设置的偶极子天线的长度和极化方向有关。这个新方法不需要任何优化程序,可以大大简化设计过程。

2 产生空间球形聚焦光斑的方法

图1给出了创建具有规定距离和空间方向的球形聚焦光斑的示意图。其中图1(a)是4Pi聚焦系统,它由两个相对的具有相同焦点的高数值孔径(NA)物镜构成,将偶极子天线置于焦点处,并设置其极化方向,如图1(b)所示。偶极子天线的位矢量用 (L, θ_0, φ_0) 表示,其中, L 表示天线的长度, θ_0 为偶极子天线方向与光轴(z 轴)正方向的夹角, φ_0 为空间偶极子天线在 xy 平面的投影与 x 轴正方向的夹角。来自空间偶极子天线的辐射场被两个相同的物镜完全收集并准直到瞳孔平面,然后用相对相差 π 相位的光将天线辐射场反转,并强聚焦在焦点区域。

用 r' 表示偶极子天线上的点与原点的距离,当 $|r'| < L/2$ 时,空间偶极子天线的电流分布^[21]为

收稿日期: 2023-10-20; 修回日期: 2023-11-20; 录用日期: 2023-11-30; 网络首发日期: 2023-12-12

基金项目: 国家自然科学基金(12274281, 61108010)、上海市自然科学基金(16ZR1411600)

通信作者: *yanfangyang@shu.edu.cn

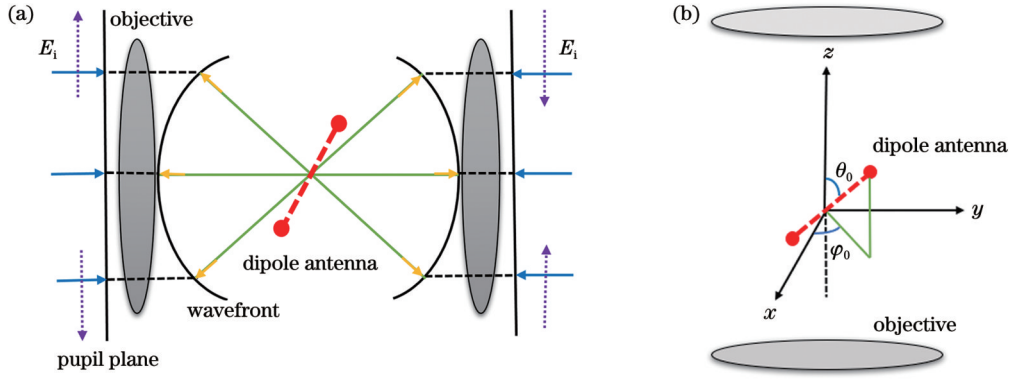


图 1 产生空间球形聚焦光斑方法的示意图。(a)4Pi 聚焦系统；(b)空间偶极子天线

Fig. 1 Schematic diagram of method for generating spatial spherical focused spots. (a) 4Pi focusing system; (b) spatial dipole antenna

$$I(r') = I_m \sin \left[k \left(\frac{L}{2} - |r'| \right) \right], \quad (1)$$

式中： k 是波数；在天线的出入口处，电流值为 $I_m \sin(kL/2)$ 。天线的矢位函数定义^[22]为

$$\mathbf{A} = \mathbf{e}_r \mu_0 I_m \frac{e^{-ibr}}{4\pi r} \int_{-L/2}^{L/2} \sin \left[k \left(\frac{L}{2} - |r'| \right) \right] e^{i\mathbf{r}' \cdot \mathbf{e}_r} d\mathbf{r}', \quad (2)$$

式中： μ_0 表示真空中的磁导率； r 为原点到空间场点的距离； \mathbf{e}_r 和 \mathbf{r}' 分别为偶极子天线的单位矢量和矢量； \mathbf{e}_r 为空间坐标的单位矢量。

$$\mathbf{r}' = r' (\sin \theta_0 \cos \varphi_0 \mathbf{e}_x + \sin \theta_0 \sin \varphi_0 \mathbf{e}_y + \cos \theta_0 \mathbf{e}_z), \quad (3)$$

$$\mathbf{e}_r = \sin \theta \cos \varphi \mathbf{e}_x + \sin \theta \sin \varphi \mathbf{e}_y + \cos \theta \mathbf{e}_z. \quad (4)$$

引入 $C(\theta, \varphi)$ 表征 $\mathbf{e}_r \cdot \mathbf{e}_r$ ：

$$C(\theta, \varphi) = \sin \theta_0 \cos \varphi_0 \sin \theta \cos \varphi + \sin \theta_0 \sin \varphi_0 \sin \theta \sin \varphi + \cos \theta_0 \cos \theta. \quad (5)$$

矢位函数可以进一步写成

$$\mathbf{A} = \mu_0 I_m \frac{e^{-ibr}}{2\pi r k} \frac{\cos \left(\frac{kL}{2} \right) - \cos \left[\frac{kL}{2} \cdot C(\theta, \varphi) \right]}{[C(\theta, \varphi) + 1] \cdot [C(\theta, \varphi) - 1]} \mathbf{e}_r. \quad (6)$$

根据电磁辐射理论，天线辐射场表示^[22]为

$$\mathbf{E} = -i\omega \left[(\mathbf{A} \cdot \mathbf{e}_\theta) \mathbf{e}_\theta + (\mathbf{A} \cdot \mathbf{e}_\varphi) \mathbf{e}_\varphi \right], \quad (7)$$

式中， \mathbf{e}_θ 和 \mathbf{e}_φ 分别为 θ 和 φ 方向的单位矢量。空间偶

极子天线辐射的总场 \mathbf{E}_{DA} 推导为

$$\mathbf{E}_{DA} = D \cdot AF(\theta, \varphi) \cdot [S(\theta, \varphi) \mathbf{e}_\theta + T(\varphi) \mathbf{e}_\varphi], \quad (8)$$

$$D = i\omega \mu_0 I_m \frac{e^{-ibr}}{2\pi r k}, \quad (9)$$

$$AF(\theta, \varphi) = \frac{\cos \left(\frac{kL}{2} \right) - \cos \left[\frac{kL}{2} \cdot C(\theta, \varphi) \right]}{[C(\theta, \varphi) + 1] \cdot [C(\theta, \varphi) - 1]}, \quad (10)$$

$$S(\theta, \varphi) = -\sin \theta_0 \cos \varphi_0 \cos \theta \cos \varphi - \sin \theta_0 \sin \varphi_0 \cos \theta \sin \varphi + \cos \theta_0 \sin \theta, \quad (11)$$

$$T(\varphi) = \sin \theta_0 \cos \varphi_0 \sin \varphi - \sin \theta_0 \sin \varphi_0 \cos \varphi, \quad (12)$$

式中： D 表示与辐射场形状无关的辐射场的辐射系数； $AF(\theta, \varphi)$ 是方向图因子，取决于电流的空间分布； $S(\theta, \varphi)$ 和 $T(\varphi)$ 分别是沿 θ 和 φ 方向的偶极子天线辐射场的元因子。

结合式(8)偶极子天线的辐射场和 Richards-Wolf 矢量衍射法，通过逆向求解问题，可以解析导出高 NA 物镜瞳孔平面处产生期望的球形光斑所需的入射场。瞳孔平面处输入场的空间坐标用 (ρ, φ) 表示，需要考虑物镜的投影函数将其转换到 (θ, φ) 空间。对于符合亥姆霍兹条件的物镜，投影函数为 $P(\theta) = (\sqrt{\cos \theta})^{-3}$ ，因此，瞳孔面处所需的输入场 \mathbf{E}_i 表示为

$$\mathbf{E}_i(\rho, \varphi) = \frac{\mathbf{E}_{DA}}{P(\theta)} = \frac{D \cdot AF(\theta, \varphi)}{(\sqrt{\cos \theta})^{-3}} [S(\theta, \varphi) \cos \varphi - T(\varphi) \sin \varphi] \mathbf{e}_x + [S(\theta, \varphi) \sin \varphi + T(\varphi) \cos \varphi] \mathbf{e}_y. \quad (13)$$

然后，反向传播，从瞳孔平面的输入场 $\mathbf{E}_i(\rho, \varphi)$ 开始，利用 Richards-Wolf 矢量衍射积分理论可以得到对应的强聚焦场 $\mathbf{E}(r, \phi, z)$ ^[23-24]为

$$\mathbf{E}(r, \phi, z) = -\frac{i}{\lambda} \int_0^\alpha \int_0^{2\pi} \mathbf{E}_i(\rho, \varphi) P(\theta) e^{iB} \sin \theta d\theta d\varphi, \quad (14)$$

式中：

$$B = k[r \sin \theta \cos(\varphi - \phi) + z \cos \theta]; \quad (15)$$

$$\alpha = \arcsin(NA/n). \quad (16)$$

下面可以通过计算上述分析的表达式，在 4Pi 聚焦系统的焦体积中创建规定空间方向和距离的球形聚焦光斑。

3 数值模拟结果与分析

为了简化计算，设置系数 D 归一化为 1。为了收

集空间偶极子天线的整个辐射场,最大辐射角为 $\alpha = \pi/2$, 对应的数值孔径 $NA = 1$, 空间折射率 $n = 1$ 。其他参数为波长 $\lambda = 632.8 \text{ nm}$, 透镜的焦距 $f = 1 \text{ mm}$ 。首先,分析偶极子天线长度 L 与产生球形聚焦光斑个数的关系。图 2 给出的是保持空间方向 ($\theta_0 = 45^\circ$, $\varphi_0 = 45^\circ$) 不变,设置天线长度 $L = 4.5\lambda, 5\lambda, 5.5\lambda, 6\lambda, 6.5\lambda, 7\lambda$ 时在 r - z 平面的总场分布。可以看出,当 L 为

半波长的奇数倍时,在设置的空间方向形成了以焦点为中心对称的两个强度相同的光斑。当 L 为半波长的偶数倍时,形成三个光斑,焦点处形成一个强度大的光斑和以焦点处光斑对称的两个强度较小的光斑。可以计算出空间光斑之间的距离等于设置的偶极子天线的长度,因此,通过改变参数 L 可以很容易地实现空间光斑距离的改变。

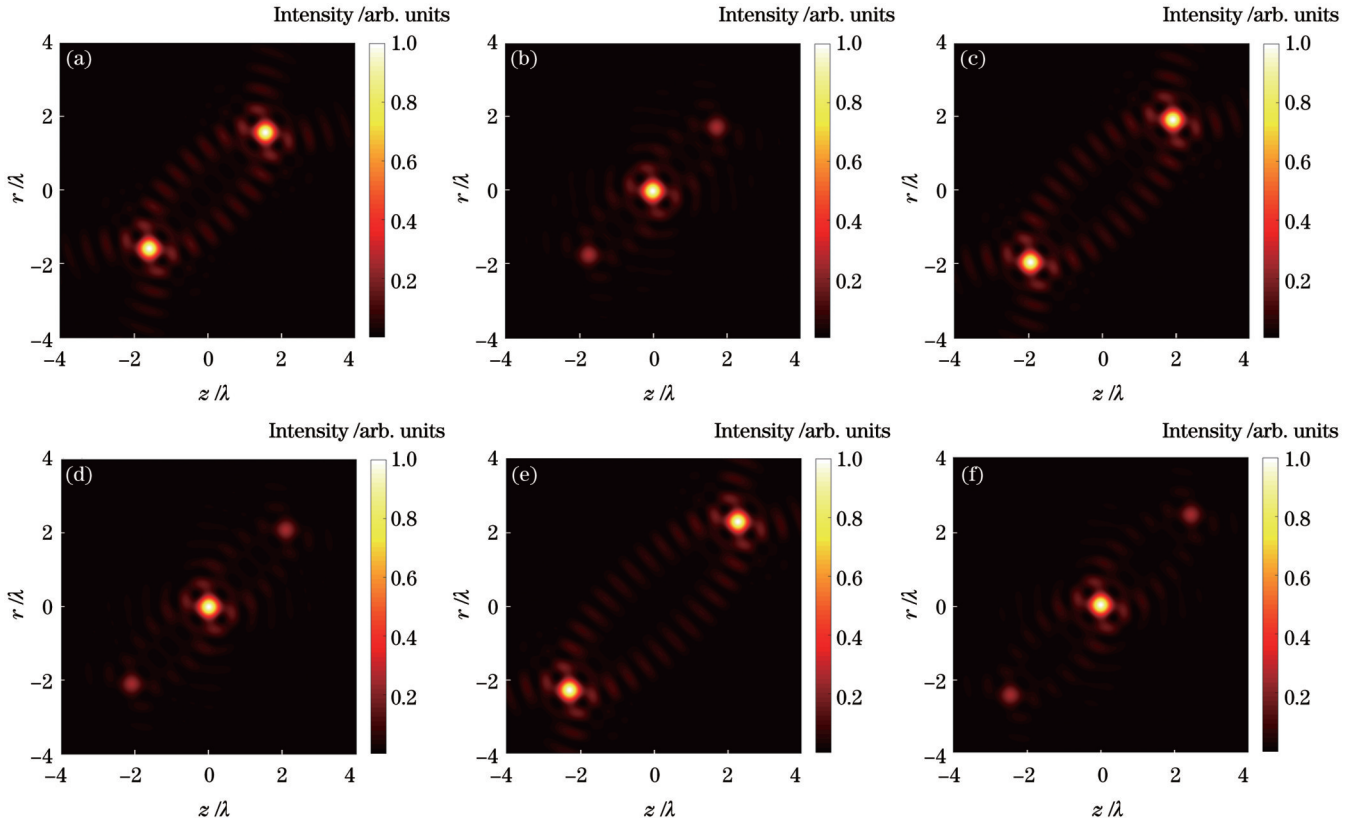


图 2 创建可控长度的空间光斑。(a) $L = 4.5\lambda$; (b) $L = 5\lambda$; (c) $L = 5.5\lambda$; (d) $L = 6\lambda$; (e) $L = 6.5\lambda$; (f) $L = 7\lambda$

Fig. 2 Creating controllable length spatial light spots. (a) $L = 4.5\lambda$; (b) $L = 5\lambda$; (c) $L = 5.5\lambda$; (d) $L = 6\lambda$; (e) $L = 6.5\lambda$; (f) $L = 7\lambda$

为了说明创建的是尺寸相同的球形聚焦光斑,本文给出了相应图 2(a)~(d) 中的光斑中心沿着 z 轴和 r 轴方向的总强度的变化线图,如图 3 所示。可以看出,每个光斑沿 z 方向和 r 方向曲线完全重合,说明每个光斑均是球形的。同时表明所有的球形聚焦光斑的尺寸是相同的,半峰全宽 (FWHM) 均等于 0.459λ 。

下面给出特例来说明所提方法的有效性和灵活性。设置偶极子天线的极化方向分别为 $(\theta_0, \varphi_0) = (90^\circ, 0^\circ), (90^\circ, 90^\circ), (0^\circ, 0^\circ)$, 即得到沿 x, y, z 轴的球形聚焦光斑,如图 4 所示。图中的第一行和第二行分别是 $L = 4.5\lambda, I = 0.5I_{\max}$ 和 $L = 5\lambda, I_1 = 0.2I_{\max}, I_2 = 0.4I_{\max}$ 的三维等值面图。分析发现,第一行两个光斑之间的距离为 4.5λ , 第二行最远的两个光斑之间的距离为 5λ , 即球形聚焦光斑之间的空间距离仅由偶极天线的长度决定。球形聚焦光斑的空间方向沿

x, y, z 轴,与相应的空间偶极子天线的极化方向相同。

为了进一步论证所提出方法的灵活性,下面创建任意空间方向的球形聚焦光斑,如图 5 所示。其中相关参数设置为 $L = 4.5\lambda, (\theta_0, \varphi_0) = (25^\circ, 15^\circ), (40^\circ, 110^\circ), (70^\circ, 150^\circ), (60^\circ, 320^\circ)$, 三维等值面取 $I = 0.5I_{\max}$ 。可以发现,球形聚焦光斑的方向与空间偶极子天线的极化方向一致,两个光斑的距离等于 4.5λ , 说明空间球形聚焦光斑的方向可以很容易地由天线参数 (θ_0, φ_0) 给定。并且空间球形聚焦光斑的距离且仅依赖于天线的长度,因此,通过改变参数 L 可以很容易地实现球形聚焦光斑距离的长短,这与图 2 生成的平面球形聚焦光斑的结论相同。

生成上述空间球形聚焦光斑所需的归一化瞳孔平面中的输入场 $\mathbf{E}_i(\rho, \varphi)$ 可由式 (13) 计算。可知输入场结构与天线参数 (θ_0, φ_0) 有关,因此需要分别考虑这两

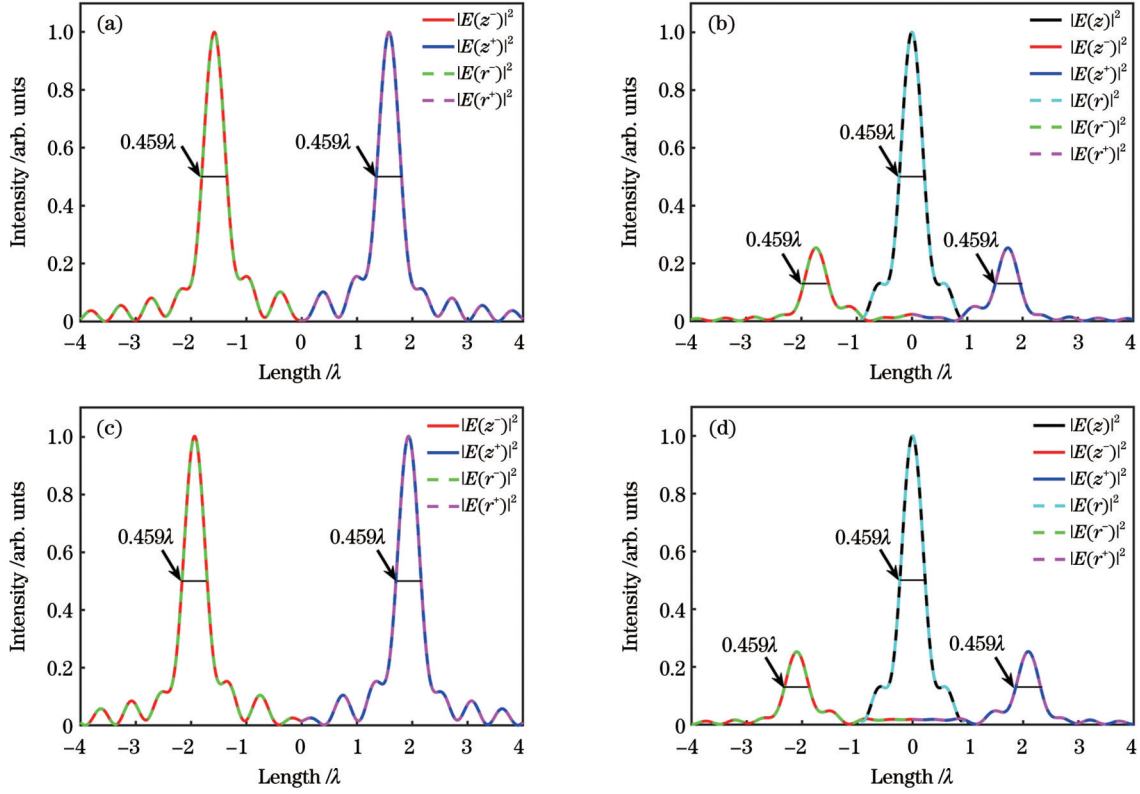


图 3 沿着 z 轴和 r 轴的总强度的线图。(a) $L = 4.5\lambda$; (b) $L = 5\lambda$; (c) $L = 5.5\lambda$; (d) $L = 6\lambda$

Fig. 3 Plots of total intensity along z and r axes. (a) $L = 4.5\lambda$; (b) $L = 5\lambda$; (c) $L = 5.5\lambda$; (d) $L = 6\lambda$

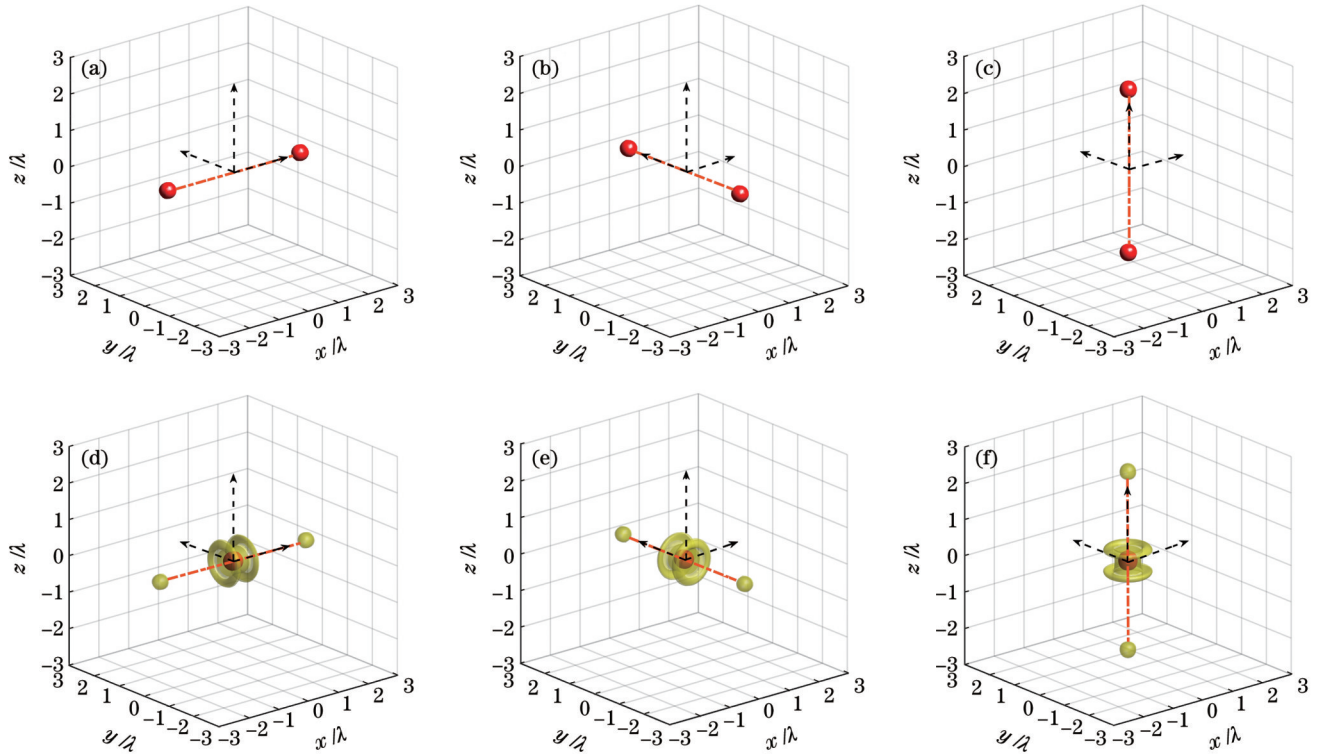


图 4 生成光轴方向的球形聚焦光斑, 其中, 第一行 $L = 4.5\lambda$, 第二行 $L = 5\lambda$ 。(a)、(d) 沿 x 轴; (b)、(e) 沿 y 轴; (c)、(f) 沿 z 轴

Fig. 4 Generating spherical focused spots in direction of optical axis, where in first row $L = 4.5\lambda$ and in second row $L = 5\lambda$.

(a), (d) Along x -axis; (b), (e) along y -axis; (c), (f) along z -axis

个参数对输入场的影响。图 6 给出了 $L = 4\lambda$, 固定 $\theta_0 = 45^\circ$, 改变 φ_0 分别为 $0^\circ, 45^\circ, 135^\circ, 180^\circ, 225^\circ, 315^\circ$ 来

形成空间球形聚焦光斑所需的输入场分布。从图中仔细观察发现, 输入场的图样是不变的, 仅随参数 φ_0 在

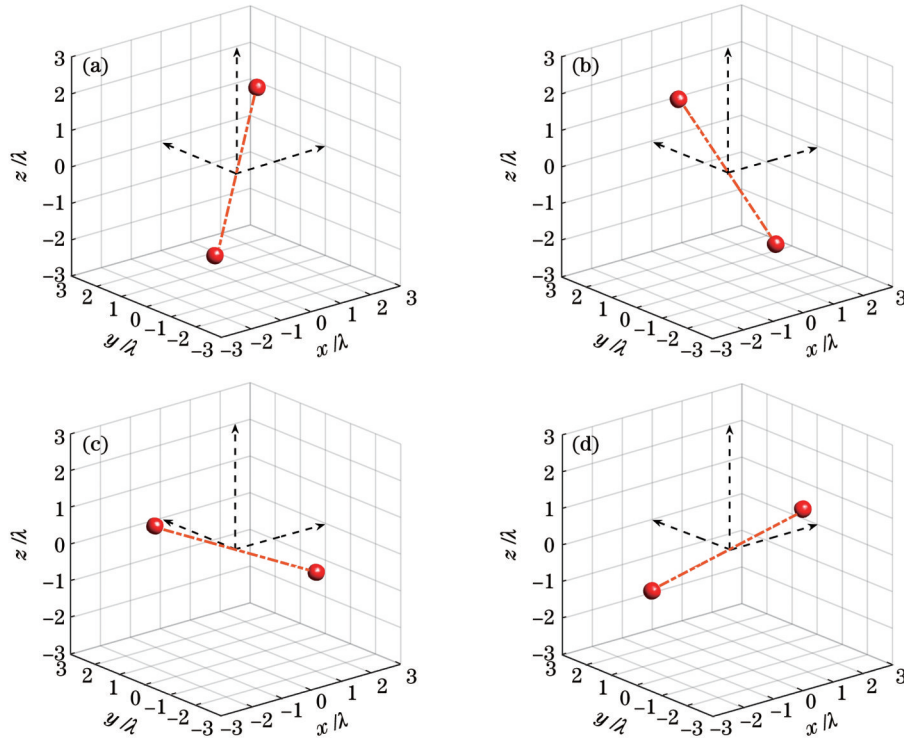


图 5 创建任意空间方向的球形聚焦光斑。(a) $(\theta_0, \varphi_0) = (25^\circ, 15^\circ)$; (b) $(\theta_0, \varphi_0) = (40^\circ, 110^\circ)$; (c) $(\theta_0, \varphi_0) = (70^\circ, 150^\circ)$; (d) $(\theta_0, \varphi_0) = (60^\circ, 320^\circ)$

Fig. 5 Creating spherical focused spots in any spatial direction. (a) $(\theta_0, \varphi_0) = (25^\circ, 15^\circ)$; (b) $(\theta_0, \varphi_0) = (40^\circ, 110^\circ)$; (c) $(\theta_0, \varphi_0) = (70^\circ, 150^\circ)$; (d) $(\theta_0, \varphi_0) = (60^\circ, 320^\circ)$

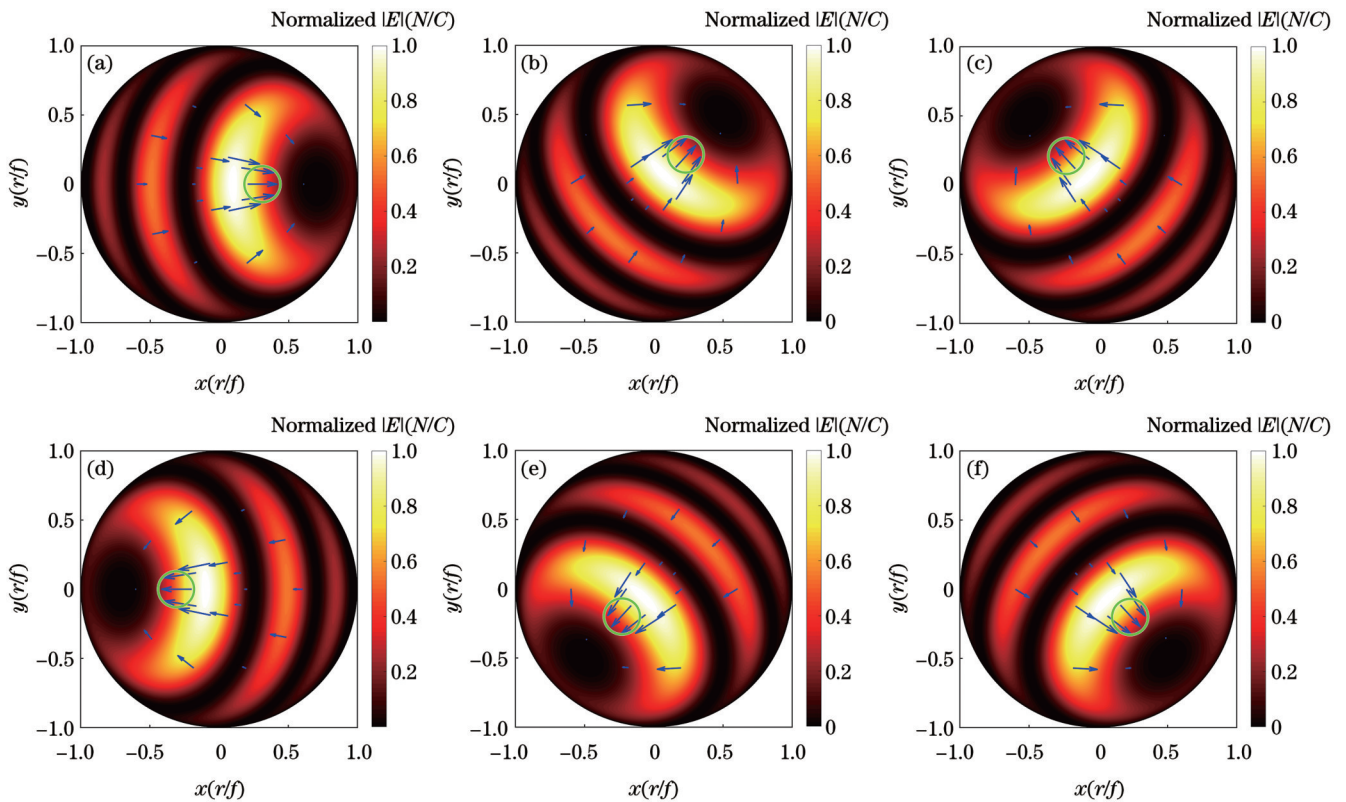


图 6 归一化的瞳孔平面中的输入场。参数: $L = 4\lambda$, $\theta_0 = 45^\circ$ 。(a)~(f) φ_0 依次为 $0^\circ, 45^\circ, 135^\circ, 180^\circ, 225^\circ, 315^\circ$

Fig. 6 Normalized input field in pupil plane. Parameters: $L = 4\lambda$, $\theta_0 = 45^\circ$. (a)–(f) φ_0 are $0^\circ, 45^\circ, 135^\circ, 180^\circ, 225^\circ$, and 315° , respectively

x - y 平面发生旋转。通过计算发现,从 x 轴测得的最大强度位置的偏振角(图中用圆圈标注)等于 φ_0 。另一种情况,取 $L = 4\lambda$ 和 $\varphi_0 = 60^\circ$ 参数不变,输入场随辐射角 θ_0 参数的变化,如图7所示。可以看出,在最大强度区域(图中用圆圈标注),偏振方向不会随辐射角 θ_0 发生变化,这是因为偏振方向仅与 φ_0 有关,固定 $\varphi_0 =$

60° ,则所有图中最大强度区域的偏振方向均与 x 轴的夹角为 60° 。参数 θ_0 与 $\pi - \theta_0$ 对应的输入场分布关于原点对称,如图7(a)和7(d)、7(b)和7(e)、7(c)和7(f)所示。当 $\theta_0 = 0^\circ$ 和 180° 时,输入场为圆环形分布,偏振分布呈径向偏振,这与传统的产生 z 轴的球形聚焦光斑的结论是一致的^[16]。

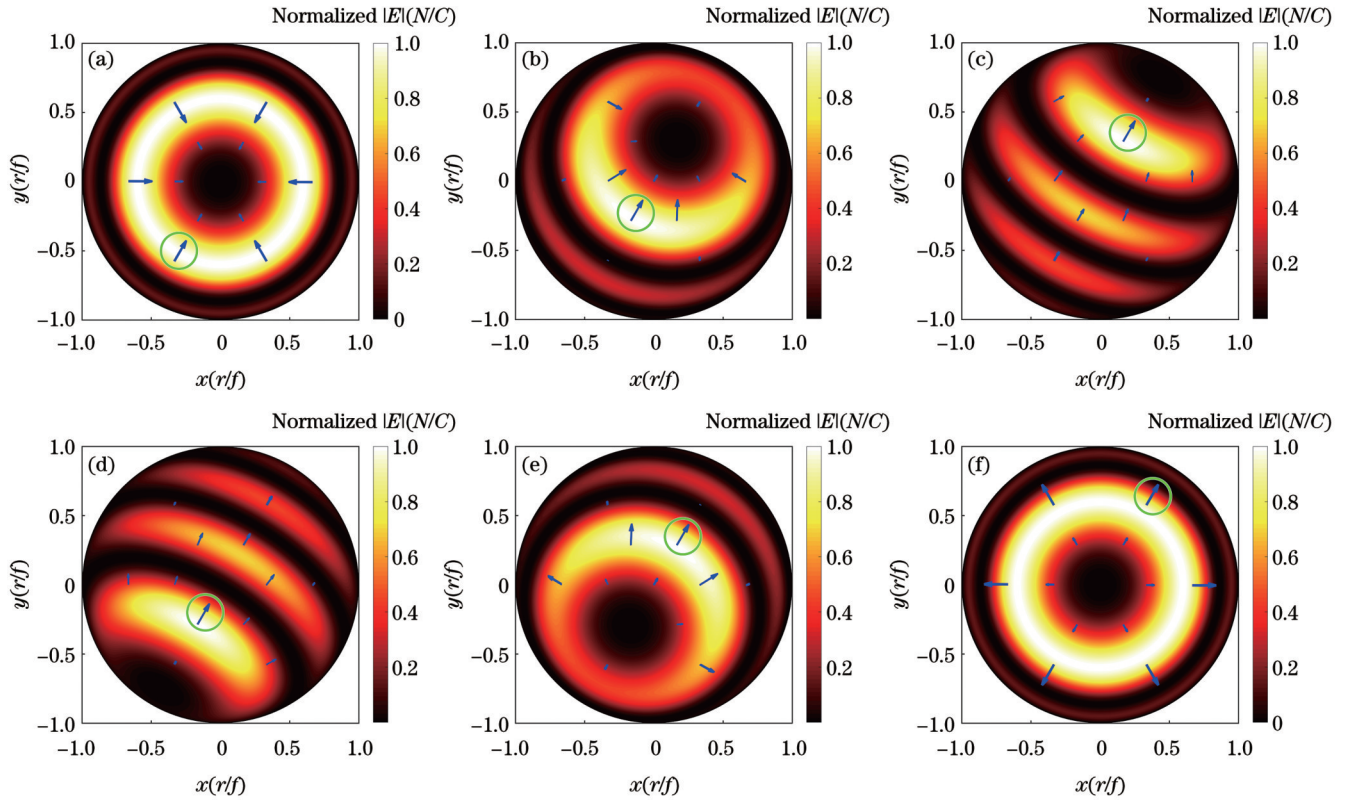


图7 归一化的瞳孔平面中的输入场。参数: $L = 4\lambda$, $\varphi_0 = 60^\circ$ 。(a)~(f) θ_0 依次为 $0^\circ, 20^\circ, 60^\circ, 120^\circ, 160^\circ, 180^\circ$

Fig. 7 Normalized input field in pupil plane. Parameters: $L = 4\lambda$, $\varphi_0 = 60^\circ$. (a)–(f) θ_0 are $0^\circ, 20^\circ, 60^\circ, 120^\circ, 160^\circ$, and 180° , respectively

4 结 论

本文介绍了一种简单、灵活的方法,创建规定长度和空间方向可控的球形聚焦光斑。通过将虚拟偶极子天线辐射的电磁场反向聚焦在4Pi聚焦系统的焦点上,可以方便地获得具有规定特性的空间球形聚焦光斑。模拟计算结果证实了球形聚焦光斑之间的距离是可变的,仅与天线长度 L 有关;球形聚焦光斑的空间方向是可调的,仅与天线参数(θ_0, φ_0)有关。并且,光学天线产生的所有球形聚焦光斑的大小是一样的,FWHM约为 0.459λ 。在这里产生的空间球形光斑可以全自由度地精准多点捕获空间纳米粒子,在光学微操控方面具有潜在的应用价值。

参 考 文 献

[1] Ashkin A, Dziedzic J M, Bjorkholm J E, et al. Observation of a single-beam gradient force optical trap for dielectric particles[J]. Optics Letters, 1986, 11(5): 288-290.

[2] 巩凡, 任煜轩. 激光双光镊在单分子生物物理中的研究进展[J]. 中国激光, 2023, 50(15): 1507402.
Gong F, Ren Y X. Advances in laser dual-trap optical tweezers in single-molecule biophysics[J]. Chinese Journal of Lasers, 2023, 50(15): 1507402.

[3] 肖雨晴, 史阳, 李宝军, 等. 基于锥形光纤光镊的细胞操控与神经调控[J]. 中国激光, 2023, 50(15): 1507302.
Xiao Y Q, Shi Y, Li B J, et al. Cell manipulation and neuron regulation based on tapered optical fiber tweezers[J]. Chinese Journal of Lasers, 2023, 50(15): 1507302.

[4] Ling L, Zhou F, Huang L, et al. Perturbation between two traps in dual-trap optical tweezers[J]. Journal of Applied Physics, 2011, 109(8): 083116.

[5] Jauffred L, Richardson A C, Oddershede L B. Three-dimensional optical control of individual quantum dots[J]. Nano Letters, 2008, 8(10): 3376-3380.

[6] Chen Y F, Serey X, Sarkar R, et al. Controlled photonic manipulation of proteins and other nanomaterials[J]. Nano Letters, 2012, 12(3): 1633-1637.

[7] Grier D G. A revolution in optical manipulation[J]. Nature, 2003, 424(6950): 810-816.

[8] Svoboda K, Block S M. Optical trapping of metallic Rayleigh particles[J]. Optics Letters, 1994, 19(13): 930-932.

[9] Hansen P M, Bhatia V K, Harrit N, et al. Expanding the

- optical trapping range of gold nanoparticles[J]. *Nano Letters*, 2005, 5(10): 1937-1942.
- [10] Vicente O C, Caloz C. Bessel beams: a unified and extended perspective[J]. *Optica*, 2021, 8(4): 451-457.
- [11] Wang J M, Chen W B, Zhan Q W. Creation of uniform three-dimensional optical chain through tight focusing of space-variant polarized beams[J]. *Journal of Optics*, 2012, 14(5): 055004.
- [12] 章红顺, 覃亚丽, 郑欢, 等. 基于 4Pi 聚焦系统的圆柱矢量涡旋光束的焦场调控[J]. *光学学报*, 2022, 42(13): 1326002.
Zhang H S, Qin Y L, Zheng H, et al. Focal field modulation of cylindrical vector vortex beams based on 4Pi focusing system[J]. *Acta Optica Sinica*, 2022, 42(13): 1326002.
- [13] Zeng Y X, Chen M S, Huang H, et al. Generating an optical needle with prescribed length and polarization direction through reversing the radiation pattern from a spatial ULS antenna[J]. *Journal of Modern Optics*, 2021, 68(21): 1202-1210.
- [14] Wang H F, Shi L P, Lukyanchuk B, et al. Creation of a needle of longitudinally polarized light in vacuum using binary optics[J]. *Nature Photonics*, 2008, 2: 501-505.
- [15] Youngworth K S, Brown T G. Focusing of high numerical aperture cylindrical-vector beams[J]. *Optics Express*, 2000, 7(2): 77-87.
- [16] Chen W B, Zhan Q W. Creating a spherical focal spot with spatially modulated radial polarization in 4Pi microscopy[J]. *Optics Letters*, 2009, 34(16): 2444-2446.
- [17] 段慧慧, 杨艳芳, 何英, 等. 4 π 聚焦系统中衍射光学元件对聚焦场多光球结构的影响[J]. *光学学报*, 2021, 41(20): 2026001.
Duan H H, Yang Y F, He Y, et al. Influence of diffractive optical elements on multiple spherical spots in a 4 π focusing system[J]. *Acta Optica Sinica*, 2021, 41(20): 2026001.
- [18] Zhan Q W. Trapping metallic Rayleigh particles with radial polarization[J]. *Optics Express*, 2004, 12(15): 3377-3382.
- [19] Ohlinger A, Nedev S, Lutich A A, et al. Optothermal escape of plasmonically coupled silver nanoparticles from a three-dimensional optical trap[J]. *Nano Letters*, 2011, 11(4): 1770-1774.
- [20] Wang X Y, Rui G H, Gong L P, et al. Manipulation of resonant metallic nanoparticle using 4Pi focusing system[J]. *Optics Express*, 2016, 24(21): 24143-24152.
- [21] 钟顺时. 天线理论与技术[M]. 北京: 电子工业出版社, 2011: 38.
Zhong S S. *Antenna theory and techniques*[M]. Beijing: Publishing House of Electronics Industry, 2011: 38.
- [22] Stutzman W L, Thiele G A. *Antenna theory and design*[M]. 2nd ed. New York: Wiley, 1998: 28-29.
- [23] Richards B, Wolf E. Electromagnetic diffraction in optical systems. II. Structure of the image field in an aplanatic system [J]. *Proceedings of the Royal Society of London Series A Mathematical and Physical Sciences*, 1959, 253(1274): 358-379.
- [24] Hell S W, Lindek S, Stelzer E H K. Enhancing the axial resolution in far-field light microscopy: two-photon 4Pi confocal fluorescence microscopy[J]. *Journal of Modern Optics*, 1994, 41(4): 675-681.

Generation of Spatial Spherical Focused Spots Based on Reverse Radiation of Dipole Antenna

Wang Junjie, Yang Yanfang*, He Ying, Li Qi, Wang Kunfeng

Department of Physics, College of Sciences, Shanghai University, Shanghai 200444, China

Abstract

Objective To solve the problem that the traditional method can only produce spherical focused spots along the optical axis, we propose a method to generate spherical focused spots in any arbitrary spatial direction in a 4Pi focusing system, which consists of two opposing high numerical aperture objective lenses with the same focus. Spherical focused spots with equivalent three-dimensional spatial resolution have important applications in optical microscopy and metal particle capture. In particular, these spots can trap metal particles at resonant wavelengths, which is because the enhanced axial gradient force and the symmetry of the 4Pi focusing system can offset the axial scattering and absorption forces, making it possible to stabilize the trapping of resonant metal particles and precisely control the motion trajectory of metal particles. Spherical focused spots should be generated at any spatial position to capture resonant metal particles at arbitrary spatial positions. To our knowledge, this is the first time that controllable spherical focused spots can be obtained at an arbitrary spatial position. The proposed method features greater flexibility than traditional approaches, making it highly valuable for applications involving nanoparticle capture at arbitrary spatial locations.

Methods We present a method to generate spherical focused spots with the specified spatial direction and spacing in a 4Pi focusing system using dipole antenna radiation fields generated by de-focusing. The method involves placing the spatial dipole antenna with predefined lengths and polarization direction at the focal point of the 4Pi focusing system and solving the inverse problem to determine the input field on the objective pupil plane that generates spherical focused spots. By utilizing the field on the pupil plane and selecting the appropriate length of the dipole antenna, spatial spherical focused spots can be obtained.

Results and Discussions Firstly, the number of generated spatial spherical focused spots is related to odd or even

multiple of half wavelength (Fig. 2). When the length of the dipole antenna L is an odd multiple of half wavelength, two same intensity spherical spots symmetrical at the center of the focus are formed in the set spatial direction. When L is an even multiple of half wavelength, three spherical focused spots with the equal size are formed, with one high-intensity spot at the focus and two lower-intensity spots symmetrically arranged. Since the distance between spatial spherical focused spots is calculated to be equal to L , the distance of spatial spherical focused spots can be easily adjusted by changing the parameter L . Meanwhile, arbitrary spatial directions of spherical focused spots are created to demonstrate the flexibility of the proposed method (Figs. 4 and 5). It is observed that the direction of the spherical focused spots is consistent with the polarization direction of the dipole antenna. Finally, we investigate the normalized input field $\mathbf{E}_i(\rho, \varphi)$ required to create the spatial spherical focused spots (Figs. 6 and 7). It is evident that the polarization direction of the input field is determined by the dipole antenna parameter φ_0 , and the dipole antenna parameter θ_0 determines the spatial rotation angle of the input field.

Conclusions We present a simple and flexible method for generating spherical focused spots of prescribed length and controllable spatial orientation. By focusing the electromagnetic field radiated by a virtual dipole antenna in reverse at the focal point of a 4Pi focusing system, spherical focused spots with specified characteristics can be conveniently obtained. The simulation results show that the number of spherical focused spots is related to odd or even multiple of half a wavelength, and the distance between spherical focused spots is adjustable and only depends on the antenna length L , while the spatial direction of spherical focused spots is controllable and depends on the antenna parameters (θ_0, φ_0) . Furthermore, all spherical focused spots generated by the optical antennas are of the same size, with a full width at half maximum (FWHM) of 0.459λ . The generated spatial spherical focused spots have potential applications in precise multi-point trapping of spatial nanoparticles with full degrees of freedom, showing broad prospect in optical micro-manipulation.

Key words physical optics; spherical focused spots; dipole antenna; 4Pi focusing system